Dependence of Arc Interrupting Capability on Spatial Distribution of Airflow Velocity in Air-Blast Flat-Type Quenching Chamber

Yasunobu Yokomizu, *Member, IEEE,* Toshiro Matsumura, *Member, IEEE,* Akiji Matsuda, and Hideyuki Ohno

***Abstract*—The dependence of an interrupting capability on the spatial distribution of airflow velocity was investigated in an air-blast flat-type quenching chamber. To obtain a various distribution of airflow velocity, the axial position of a nozzle and the inlet width of the nozzle were varied. For each of the axial positions and each of the inlet widths, arc interruption tests for ac currents were performed to measure the interrupting capability. Furthermore, the distribution of airflow velocity in the quenching chamber was calculated intentionally in the absence of the arc. From the test and calculation results, we found out a definite relationship between the velocity distribution and the interrupting capability.**

***Index Terms*—Airflow, arc discharges, correlation, interrupting capability, vortex.**

I. Introduction

MANY INVESTIGATIONS have been performed to understand the arc interruption process in air- and gas-blast circuit breakers. Some of the studies researched the interrupting capability of the breaker in terms of an arc conductance, arc temperature, and operating pressure [1]–[8].

As is well known, the interrupting capability of a circuit breaker adopting an axial blast of either air or SF_6 through a nozzle depends on many factors such as mass flow rate, the ratio of upstream pressure to downstream pressure, a nozzle shape, and a contact shape. However, this dependence of the interrupting capability on these factors is considered to be attributable to the following physical phenomena: these factors significantly dominate the gas-flow condition and this flow condition affects the arc properties, finally influencing the interrupting capability. On the other hand, the interrupting capability depends not only on the above factors but also on the ability to move hot gases out of the arcing chamber after interruption. This dependence is also considered to appear on the basis of the physical phenomenon that the gas-flow condition affects the ability to eject the hot gases, then dominate the interrupting capability.

From the above point of view, the interrupting capability of the circuit breaker seems to have distinct correlation to the gas-flow condition in the arc quenching chamber. However, little work has been done to investigate the relationship between the arc interrupting capability and the gas-flow condition. The objective of the present work is to research the dependence of the interrupting capability on the spatial distribution of the gas-flow velocity. A scaled-down flat-type air-blast quenching chamber was used. Varying the axial position of a nozzle and the width of the nozzle inlet enables obtaining different distributions of airflow velocities in the quenching chamber. For each axial position and inlet width, a number of arc interruption tests were carried out to measure an interrupting capability of the quenching chamber. Furthermore, the spatial distribution of the airflow velocity in the arc quenching chamber was calculated theoretically. This calculation was intentionally made in the absence of the arc. From the results of the calculations and the interruption tests, we found a relationship between the interrupting capability and the distribution of the airflow velocity.

The distribution in the absence of the arc differs from that in the presence of the arc, since physical quantities, such as a mass density and a viscosity of the air, depend on the temperature. However, we calculated the distribution of the airflow velocity in the absence of the arc on the basis of two principal reasons. First, the fact that even the airflow behavior for case without the arc has a distinct relationship with the interrupting capability is of great worth in the research field of circuit breakers. This is because the relationship found in the present work is a great advantage in that a nozzle shape, producing high interrupting capability, is determined without complicated calculations for arc behavior. Second, the calculation for the case in the presence of the arc frequently requires some procedures of assumptions and approximations to various physical factors. Thus, this situation may cause the validity of the calculation results to remain obscure. On the contrary, since there is no need for neither the assumptions nor approximations, the calculation for the case without the arc is considered to provide exact velocities.

II. Interruption Test

A. Experimental Setup

We have so far used a scaled-down flat-type air-blast quenching chamber to research an arc interruption process in terms of the electron density in the arc [9]–[11]. This is because the adoption of the flat-type quenching chamber enabled us to measure the electron density by detecting the

Manuscript received November 30, 1999; revised August 2, 2002. This work was supported in part by the New Energy and Industrial Technology Development Organization of Japan.

Y. Yokomizu, T. Matsumura, and A. Matsuda are with the Department of Electrical Engineering, Nagoya University, Nagoya, 464-8603 Japan (e-mail: yokomizu@nuee.nagoya-u.ac.jp).

H. Ohno is with the Department of Electrical Engineering, Meijo University, Nagoya, 468-0073 Japan.

Digital Object Identifier 10.1109/TPWRD.2002.806687

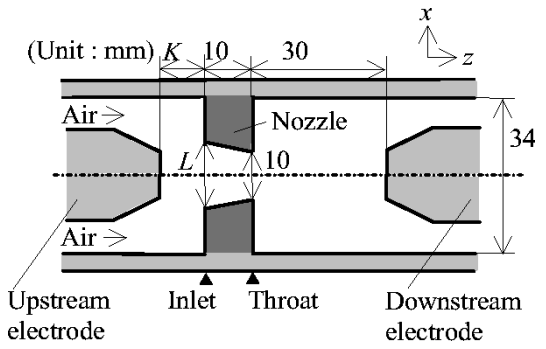

Fig. 1. Flat-type air-blast quenching chamber of 3 mm in thickness. This quenching chamber is sandwiched between two plates made of PTFE.

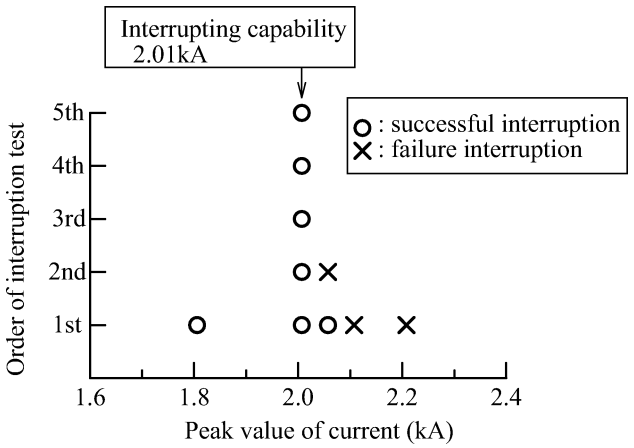

Fig. 2. Result of interruption test for distance $K = 10$ mm between upstream electrode and nozzle throat and width $L = 15$ mm of nozzle inlet.

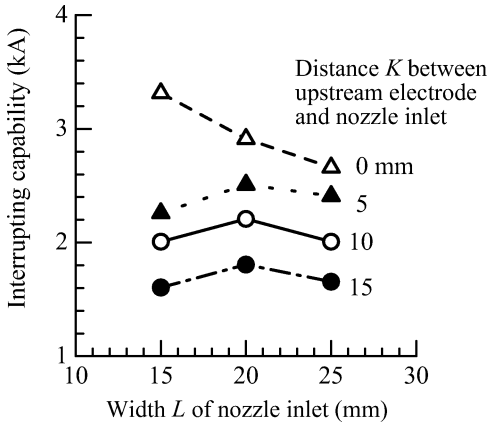

Fig. 3. Interrupting capability as a function of width L of nozzle inlet for different distances K between upstream electrode and nozzle inlet.

amplitude of 70-GHz microwave transmitted through the arc plasma [12]–[14]. The present work also used this quenching chamber since a number of interruption tests were capable of being performed without any difficulty. Fig. 1 illustrates the schematic diagram of the flat-type air-blast quenching chamber that is 3 mm thick. This chamber was sandwiched between two plates made of polytetrafluoroethylene (PTFE). Graphite was used as an electrode material. This is because the graphite electrode is rarely melted for the transient ac current arc so that the arc is almost free from contamination of electrode vapor [15], [16]. The gap length between the electrodes was kept to be 50 mm.

Generally speaking, most breakers used in a power transmission system do not have a fixed set of contacts so the geometry is always changing with the elapse of the time in the opening process of the contacts. This means that gas-flow velocity distribution also varies with the passage of the time. However, in the present research, the fixed set of the electrodes was intentially adopted from the fundamental point of view to focus on the gas-flow velocity distribution under stationary state.

In Fig. 1, dark-shaded portions represent a nozzle made of PTFE. This nozzle is what is called orifice type, having a length of 10 mm and a throat width of 10 mm. To obtain various distributions of airflow velocities in the quenching chamber, we varied the axial position of the nozzle, namely the distance K between the tip of an upstream electrode and a nozzle inlet, to be 0, 5, 10, and 15 mm. In addition, for each distance K, the width L of the nozzle inlet was also varied to be 15, 20, and 25 mm.

In this quenching chamber, air was supplied through tubes besides the electrode on the left-hand side to blow an arc in an axial direction at a rate of 2.5×10^{-3} m^3/s ($= 150\ \ell$/min). The blast air passed through the nozzle, then leaving the chamber through holes besides the electrode on the right-hand side. Pressure in the quenching chamber was kept at 0.1 MPa throughout the experiments.

B. Interrupting Capability

A damping sinusoidal current with a frequency of 60 Hz was supplied from a capacitor bank of 3580 μF through a reactor of 1.9 mH. Adjusting the charge voltage to the capacitor bank generated the current with the peak value I_p of the first half cycle in the range of 1.4 to 3.4 kA. The increase in I_p raised the rate of rise of recovery voltage, $rrrv$, immediately after the first current zero proportionally. This relation is expressed by

$$rrrv = 0.999 \times 10^5 \times I_p. \tag{1}$$

Interruption tests were carried out to measure the interrupting capability for each K and L. In the tests, whether the arc quenching chamber interrupted the ac current at the first current zero or not was recorded. Fig. 2 shows the result of the interruption test for various I_p in case of the distance K of 10 mm and the inlet width L of 15 mm. In this figure, an open circle and a cross denote the successful and failure interruptions, respectively. As seen in Fig. 2, the quenching chamber failed in interrupting the ac currents with a peak value I_p of 2.21 or 2.11 kA at the first interruption test. The quenching chamber also failed in interrupting the ac current with a peak value I_p of 2.06 kA at the second interruption test. However, the quenching chamber succeeded in successively interrupting the ac current with I_p of 2.01 kA five times. On the basis of the test results, we regarded the interrupting capability for $K = 10$ mm and $L = 15$ mm as 2.01 kA.

Similar interruption tests were performed for different K and L. Fig. 3 represents the measured interrupting capability as a function of the width L of the nozzle inlet for different distances

K. For K of 0 mm, an increase in L from 15 to 25 mm leads a reduction in the interrupting capability from 3.31 to 2.66 kA. For K of 5, 10, and 15 mm, a rise in L from 15 and 20 mm increases the interrupting capability, while a further growth in L from 20 to 25 mm lessens the interrupting capability. On the other hand, an increase in K declines the interrupting capability for the same L.

III. Calculation of Spatial Distribution of Airflow Velocity

A. Distribution

As stated before, the interrupting capability varies with the distance K and the inlet width L. To interpret this variation, we calculated two-dimensional (2-D) distribution of the airflow velocity by solving the following equations of mass and momentum conservation with the aid of a computer fluid dynamic tool:

$$\frac{\partial(\rho u)}{\partial x}+\frac{\partial(\rho w)}{\partial z}=0, \tag{2}$$

$$\frac{\partial(u\rho u)}{\partial x}+\frac{\partial(w\rho u)}{\partial z}=-\frac{\partial P}{\partial x}+\frac{\partial}{\partial x}\left(2\mu\frac{\partial u}{\partial x}\right)+\frac{\partial}{\partial z}\left(\mu\frac{\partial w}{\partial x}\right)+\frac{\partial}{\partial z}\left(\mu\frac{\partial u}{\partial z}\right), \tag{3}$$

$$\frac{\partial(u\rho w)}{\partial x}+\frac{\partial(w\rho w)}{\partial z}=-\frac{\partial P}{\partial z}+\frac{\partial}{\partial z}\left(2\mu\frac{\partial w}{\partial z}\right)+\frac{\partial}{\partial x}\left(\mu\frac{\partial u}{\partial z}\right)+\frac{\partial}{\partial x}\left(\mu\frac{\partial w}{\partial x}\right), \tag{4}$$

where x and z are coordinates shown in Fig. 1. Variables u and w are x and z directional components of the flow velocity, respectively. The quantity P is an air pressure. Then ρ and μ are a mass density of 1.1774 kg/m^3 and a viscosity of 1.983×10^{-5} Pa $\cdot$ s for air at a temperature of 300 K, respectively [17], [18]. In this way, the 2-D distribution of the airflow velocity was obtained under the condition of the air temperature of 300 K, namely in the absence of the arc.

Fig. 4(a) presents the derived velocities in a general view for the distance K of 10 mm and the inlet width L of 15 mm. Fig. 4(b) and (c) show the calculated velocities in front of an upstream electrode and in a region within the nozzle, respectively. Details of the flow velocity distribution will be discussed.

B. Profile of Flow Velocity at Nozzle Throat

As is well known, physical phenomena at nozzle throat have a great influence on arc interruption performance. Thus, we paid attention to the flow velocity at the nozzle throat. Fig. 5 represents the flow velocity at the cross section of the nozzle throat as a function of a distance x from the central axis of the nozzle. This figure presents the velocities calculated for three cases as examples. Whereas moving at a velocity of approximately 90 m/s at distances around $x=3$ mm, the air for the distance K of 0 mm and the inlet width L of 20 mm flows at

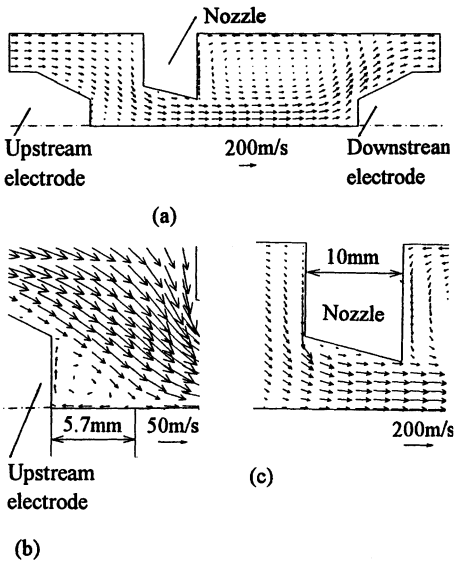

Fig. 4. Airflow velocity vectors calculated for distance $K=10$ mm from upstream electrode to nozzle throat and width $L=15$ mm of nozzle inlet under conditions of airflow rate of 2.50×10^{-3} m^3/s and air temperaure of 300 K.

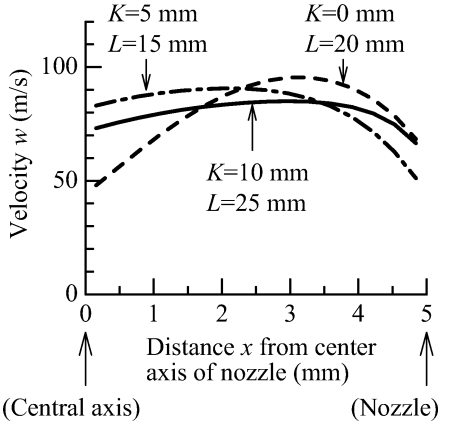

Fig. 5. Airflow velocity at a nozzle throat as a function of distance from central axis of nozzle for three cases. (Airflow rate: 2.50×10^{-3} m^3/s, air temperature: 300 K).

a lower velocity at positions more adjacent to the central axis of the nozzle. In other words, the greater part of the air flows at distances around $x=3$ mm. On the other hand, the air for $K=10$ mm and $L=25$ mm moves at almost uniform velocity over the cross section of the nozzle throat. In comparison with the case for $K=10$ mm and $L=25$ mm, the velocity for $K=5$ mm and $L=15$ mm is high at the locations near the central axis, but are low at the positions in the vicinity of the nozzle wall. In other words, the majority of the air for $K=5$ mm and $L=15$ mm flows at the locations that are somewhat more adjacent to the central axis than the nozzle wall.

As described before, the profiles of the airflow velocity at the nozzle throat markedly depend on the distance K and inlet width L. We defined the following expression to quantitate the profile of the mentioned velocity distribution:

$$\gamma=\frac{1}{\frac{D}{2}}\int_0^{D/2}\left(1-2\frac{x}{\frac{D}{2}}\right)\frac{w(x)}{w_{av}}dx, \tag{5}$$

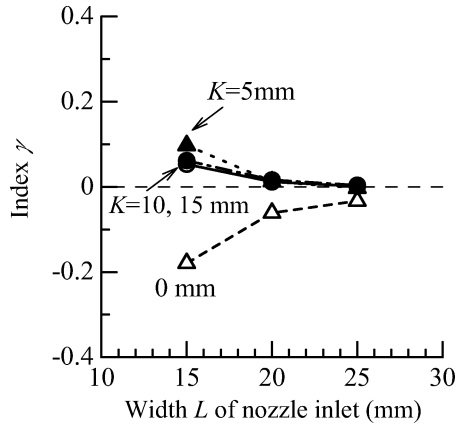

Fig. 6. Index γ of airflow-velocity profile at nozzle throat as a function of width L of nozzle inlet for different distances K between upstream electrode and nozzle inlet. (Airflow rate: 2.50×10^{-3} m^3/s, air temperature: 300 K).

where D is the width of the nozzle throat, 10 mm, x is the distance from the central axis of the nozzle, w_{av} is an average value of the flow velocity at the nozzle throat, 83.3 m/s.

The physical meaning of γ may be better understood by rearranging (5) in the form

$$\gamma = 1 - 2\frac{\bar{x}}{\frac{D}{2}} \tag{6}$$

where

$$\bar{x} = \frac{\int_0^{D/2} xw(x)\,dx}{\int_0^{D/2} w(x)\,dx}. \tag{7}$$

The quantity $\bar{x}$ is equal to the center of the airflow-velocity profile at the nozzle throat, and thus, varies in range from 0 to $D/2$ with the profile $w(x)$. Accordingly, γ declines linearly from 1 to -1 with a rise in $\bar{x}$ from 0 to $D/2$ in accordance with (6).

For instance, the entirely uniform profile of $w(x)$ results in $\bar{x}$ being $D/4$, thereby causing γ to be zero. By way of another example, the profile similar to that for $K = 0$ mm and $L = 20$ mm gives $\bar{x}$ of $D/4$ to $D/2$, thus producing γ of a negative value. In contrast, the profile similar to that for $K = 5$ mm and $L = 15$ mm causes $\bar{x}$ to be in the range from 0 to $D/4$, thus giving γ a positive value.

Fig. 6 indicates γ determined from (5) as a function of the inlet width L for different distances K. Although having a positive value for K of 5, 10, and 15 mm, γ has a negative value for $K = 0$ mm. For K of 10 and 15 mm, γ slightly decreases from approximately 0.06 to 0 with a rise in L from 15 to 25 mm. Similar dependence of γ on L is seen for K of 5 mm. However, γ for K of 0 mm markedly grows from -0.18 to -0.03 with L from 15 to 25 mm.

C. Vortex

Fig. 4(b) shows that vortex occurs in front of the upstream electrode. This vortex causes a back flow on the central axis of the quenching chamber. Fig. 7 represents the flow velocity w on the central axis of the quenching chamber as a function of axial distance from the tip of the upstream electrode. In this figure,

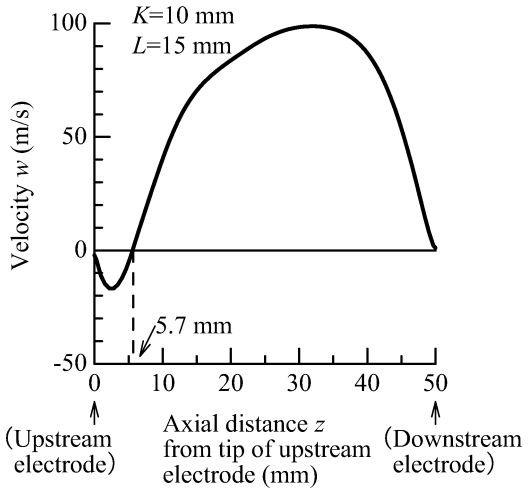

Fig. 7. Airflow velocity on central axis of quenching chamber as a function of axial distance from the tip of upstream electrode for $K = 10$ mm and $L = 15$ mm. (Airflow rate: 2.50×10^{-3} m^3/s, Air temperature: 300 K).

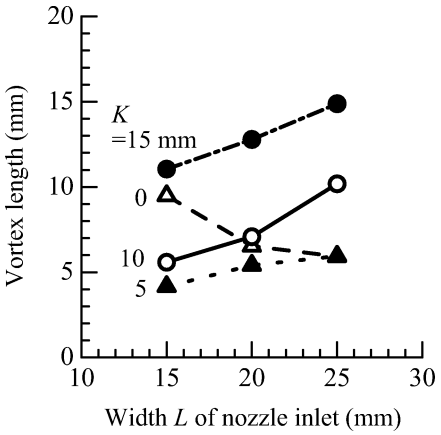

Fig. 8. Vortex length as a function of width L of nozzle inlet for different distances K between upstream electrode and nozzle inlet. (Airflow rate: 2.50×10^{-3} m^3/s, air temperature: 300 K).

the velocity is taken to be positive in case the air flows toward a downstream electrode. As seen in Fig. 7, the velocity is negative between the tip of the upstream electrode and a position 5.7 mm downstream from the tip. This negative velocity results from the back flow due to the vortex.

We paid attention to the vortex. Let us define the length ℓ of the vortex as the length of the region where the velocity is negative on the central axis of the quenching chamber. The length of the vortex is determined to be 5.7 mm in case of Fig. 7. Fig. 8 shows the obtained ℓ as a function of the inlet width L for various distances K. The vortex length for $K = 5$ mm and $L = 15$ mm is 4.2 mm, which is the lowest in comparison with those for the others K and L. The vortex length for $K = 15$ mm and $L = 25$ mm is 14.9 mm, which is 3.5× as long as that for $K = 5$ mm and $L = 15$ mm. Therefore, the vortex length significantly varies with both K and L.

IV. Dependence of Interrupting Capability on Airflow-Velocity Distribution

Fig. 9 summarizes the results shown in Figs. 3, 6, and 8. In Fig. 9, the interrupting capability measured by the interruption

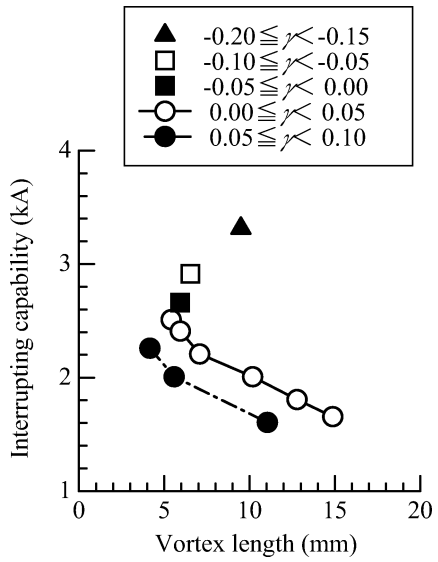

Fig. 9. Interrupting capability measured by interruption test as a function of vortex length determined by airflow-velocity calculation.

test is plotted against the vortex length calculated by airflow-velocity analysis. In addition, the plotted points are classified into five groups in accordance with the magnitude of γ. Whereas differing from the distribution in the presence of the arc, the airflow-velocity distribution described in the present paper proved from Fig. 9 to have a definite relationship to the interrupting capability of the quenching chamber. The detailed explanation is provided.

1) The interrupting capability increases with a reduction in the length of the vortex for the same γ. By way of the example, the interrupting capability rises from 1.66 to 2.51 kA with a diminution in the length of the vortex from 14.9 to 5.4 mm for γ of 0 to 0.05.
2) The interrupting capability grows with a declination in γ for the same length of the vortex. By way of the example, for the vortex length of approximately 6 mm, the interrupting capability augments from 2.01 to 2.66 kA with decreasing γ from 0.053 to -0.033.

As far as nozzles adopted in the present research are concerned, the relationships described in the items mentioned before lead to the conclusion that either a lower γ or a shorter region of the vortex in front of the upstream electrode causes the quenching chamber to have higher interrupting capability.

V. Conclusion

We investigated the interrupting capability of the flat-type air-blast quenching chamber from the viewpoint of the airflow distribution. Varying the axial position and the inlet width of the nozzle permitted obtaining various distributions of the airflow velocities. Under each condition, the interruption tests were carried out to measure the interrupting capability. Furthermore, the distribution of the airflow velocity under each condition was calculated intentionally in the absence of the arc. As a result, the interrupting capability proved to correlate with the velocity distribution of the airflow at the nozzle throat and the length of the vortex in front of the upstream electrode. The results obtained in the present work are restricted to the scaled-down quenching chamber with an interrupting capability of thousands of amperes, which is considerably lower than that in an actual full-scale circuit breaker. However, the relationship found in the present work is expected to be held for the actual full-scale circuit breaker.

References

[1] R. D. Garzon, *High Voltage Circuit Breakers—Design and Applications*. New York: Marcel Dekker, 1997, pp. 147–148.
[2] K.P. Brand, W. Egli, L. Niemeyer, K. Ragaller, and E. Shade, "Dielectric recovery of an axially blown SF6-arc after current zero: Part III–comparison of experiment and theory," *IEEE Trans. Plasma Sci*, vol. PS-10, pp. 162–172, 1982.
[3] R. E. Blundell and M. T. C. Fang, "A simplified turbulent arc model for the current-zero period of a SF_6 gas-blast circuit breaker," *J. Phys. D, Appl. Phys.*, vol. 31, pp. 561–568, 1998.
[4] G. Frind and J. A. Rich, "Recovery speed of axial flow gas-blast interrupter dependence on pressure and dI/dt for air and SF_6," *IEEE Trans. Power App. Syst.*, vol. 93, pp. 1675–1684, Sept./Oct. 1974.
[5] G. R. Jones, *High Pressure Arcs in Industrial Devices -Diagnostics and Monitoring Techniques*. Cambridge, U.K.: Cambridge University Press, 1988, pp. 202–228.
[6] A. Gleizes, M. Mitiche, and V. D. Pham, "Study of a circuit-breaker arc with self-generated flow: Part III-the post-arc phase," *IEEE Trans. Plasma Sci.*, vol. 19, pp. 12–19, Feb. 1991.
[7] T. Mori, H. Ohashi, H. Mizoguchi, and K. Suzuki, "Investigation of technology for developing large capacity and compact size GCB," *IEEE Trans. Power Delivery*, vol. 12, no. 2, pp. 747–753, Apr. 1997.
[8] T. Matsumura, W. T. Oppenlander, C. A. Schmidt-Harm, and A. D. Stokes, "Prediction of circuit-breaker performance based on a refined cybernetic model," *IEEE Trans. Plasma Sci.*, vol. PS-14, pp. 435–443, Aug. 1986.
[9] H. Ohno, H. Naganawa, T. Matsumura, and Y. Kito, "Effects of nozzle shapes on electron density distribution along the axis and on arc interruption capability observed in flat-type air-blast quenching chamber," in *Proc. 9th Int. Conf. Gas Discharges Their Applicat.*, 1988, pp. 47–50.
[10] H. Ohno, H. Naganawa, N. Kato, and Y. Kito, "Electron density distribution along the nozzle throat axis observed in flat-type air-blast quenching chambers" (in Japanese), *Trans. Inst. Electr. Eng. Jpn. B*, vol. 108-B, no. 9, pp. 423–430, 1988.
[11] H. Ohno, H. Naganawa, and Y. Kito, "Effect of air flow passage on current interruption ability verified in flat-type air-blast quenching chambers" (in Japanese), *Trans. Inst. Electr. Eng. Jpn. B*, vol. 114-B, no. 11, pp. 1168–1174, 1994.
[12] Y. Kito and H. Ohno, "Electron density measurement by sensitive cut-off attribute of incident EHF microwave in a transient narrow gap arc," in *Proc. 7th Int. Conf. Gas Discharges Their Applicat.*, 1982, pp. 529–532.
[13] H. Ohno, H. Naganawa, S. Kawakami, and Y. Kito, "Arc interruption performance in a flat quenching chamber distinguished by 70 GHz microwave diagnosis" (in Japanese), *Trans. Inst. Electr. Eng. Jpn. B*, vol. 105-B, no. 11, pp. 933–940, 1985.
[14] H. Ohno, H. Naganawa, N. Kato, and Y. Kito, "Particle composition in high temperature air contaminated by ablation gas of PTFE and its applications to electron density measurement by a microwave method" (in Japanese), *Trans. Inst. Electr. Eng. Jpn. B*, vol. 108-B, no. 4, pp. 157–164, 1988.
[15] Y. Yokomizu, T. Sakuta, and Y. Kito, "A novel approach to ac air arc interruption phenomena viewed from the electron density at current zero," *J. Phys. D, Appl. Phys.*, vol. 22, pp. 129–135, 1989.
[16] W. R. Wilson, "High-current arc erosion of electrical contact material," *Amer. Inst. Elect. Eng. Trans. PAS*, pt. 3, vol. 74, pp. 657–664, 1955.
[17] I. Tanishita, *Heat Transfer Engineering* (in Japanese) Tokyo, Shokabo, 1986, p. 310.
[18] M. I. Boulos, P. Fauchais, and E. Pfender, *Thermal Plasmas—Fundamental and Applications*. New York: Plenum , 1994, pp. 413–415.

Yasunobu Yokomizu (M'95) received the B.S., M.S., and Ph.D. degrees in electrical engineering from Nagoya University, Nagoya, Japan, in 1985, 1987, and 1991, respectively.

Currently, he is Associate Professor in the Department of Electrical Engineering at Nagoya University. He was also a Visiting Fellow in the University of Liverpool, Liverpool, U.K., from 1997 to 1998. He researches electric energy systems and their related phenomena.

Dr. Yokomizu is a member of the IEE of Japan and Japan Society of Energy and Resources.

Toshiro Matsumura (M'95) received the B.S., M.S., and Ph.D. degrees in electrical engineering from Nagoya University, Nagoya, Japan, in 1974, 1976, and 1980, respectively.

Currently, he is a Professor in the Department of Electrical Engineering at Nagoya University. He is currently involved in a study on an effective utilization of electrical energy and on high-current arc interruption phenomena.

Akiji Matsuda received the B.S. and M.S. degrees in electrical engineering from Nagoya University, Nagoya, Japan, in 1997 and 1999, respectively, where he studied high-current arc interruption phenomena.

Currently, he is with Kansai Electric Power Co., Osaka, Japan, where he has been since 1999.

Hideyuki Ohno received the B.S. degree in electrical engineering from Gifu University, Gifu, Japan, in 1965, and the Ph.D. degree in electrical engineering from Nagoya University, Nagoya, Japan, in 1989.

Currently, he is a Professor at Meijo University, Nagoya, Japan, and is involved in a study on high-current arc phenomena.